Bulletin of the Seismological Society of America, Vol. 93, No. 6, pp. 2375–2388, December 2003

On the Self-Healing Fracture Mode

by S. Nielsen and R. Madariaga

Abstract We present the analytical solution for a fundamental fracture mode in the form of a self-similar, self-healing pulse. The existence of such a fracture mode was strongly suggested by recent numerical simulations of seismic ruptures but, to our knowledge, no formal proof of their origin has been proposed yet. We present a two-dimensional, anti-plane solution for fixed rupture and healing speeds that satisfies both the wave equation and crack boundary conditions for a simple Coulomb friction law in the absence of any rate or state dependence. This solution is an alternative to the classic self-similar crack solution by Kostrov. In practice, the self-healing impulsive mode rather than the expanding crack mode is selected depending on details of fracture initiation and is thereafter self-maintained. We discuss stress concentration, fracture energy, and rupture velocity and compare them to the case of a crack. The analytical study is complemented by various numerical examples and comparisons. On more general grounds, we argue that an infinity of marginally stable fracture modes may exist in addition to the crack solution or the impulsive fracture described here.

Introduction

As initially reported by Heaton (1990), many earthquakes seem to be produced by the propagation of relatively narrow rupture pulses (see Beroza and Mikumo [1996] and references therein for several examples of short slip duration). Since then, self-healing slip pulses have also been reported in laboratory experiments (Rubio and Galeano, 1994; Anoshehpoor and Brune, 1999; Baumberger *et al.*, 2001). These self-healing ruptures do not agree with the predictions of the more classical rupture model of Kostrov (1964b) in which slip continues way behind the rupture front until stopping phases arrive from the edges of the fault.

In a number of investigations on the possible origins of self-healing rupture pulses, early healing of the fault has been attributed to the presence of strong rate weakening in the friction law, as seen, for example, in Heaton (1990), Cochard and Madariaga (1994), and Madariaga and Cochard (1994) and more recently in Zheng and Rice (1998).

Other possible origins of narrow rupture pulses have been proposed; for instance they appear in rupture propagation between dissimilar materials but only in the plane mode (Weertman, 1980; Ben-Zion and Andrews, 1998; Anoshehpoor and Brune, 1999; Cochard and Rice, 2000). In all these models pulselike rupture propagation is a consequence of the material properties of the media surrounding the faults and/or the frictional properties of the fault itself.

In addition, it appears from a number of numerical experiments that early healing can accompany the stopping phase generated at a barrier, even in the absence of any particular frictional property or material contrast. The first to illustrate this mechanism was probably Day (1982), in a 3D numerical simulation where slip was blocked outside a rectangular patch. Hints of a stable, persistently propagating pulse solution were also given in the work of Johnson (1990, 1992) for a case where a crack was blocked by a barrier at one end; similar examples were subsequently reported by Perrin *et al.* (1995). Finally, short fracture pulses can be generated in numerical models by inhomogeneity in the stress distributions, as argued by Beroza and Mikumo (1996).

Clear evidence of persistent, self-similar, and self-healing pulses was found in a number of numerical experiments by Nielsen and Carlson (2000). They showed that if the healing front was initiated at the start of rupture, healing could propagate behind the rupture and would self-maintain under a wide variety of stress and friction parameters, even at negligible levels of rate weakening in the friction. The numerical results reported by Nielsen and Carlson (2000) and previous authors pose the question of whether self-healing solutions may exist and propagate spontaneously under homogeneous stress conditions and classical Coulomb friction, as in the case of Kostrov's expanding crack (Kostrov, 1964b). In other words, do self-similar solutions other than that of Kostrov exist, and if they exist can they explain the numerical results? It seems that such solutions were not found in previous work on self-similar crack problems (see Willis [1973] and references therein for a discussion of the self-similar solutions known in the early 1970s).

Self-healing rupture pulses were investigated very early

by Yoffe (1951), who found a steady state solution for a fixed width, propagating pulse in mode I (opening mode). The pulse induced only a transient opening followed by closing, so that no net displacement was left in the wake of healing. Broberg (1978) later extended the solution to a mode II, shear fracture pulse, followed by Freund (1979), who proposed an improved solution where an undesirable stress concentration was eliminated from the healing front, in agreement with later works by Broberg (1999). In the shear models, slip is not supposed to reverse so that a final, net displacement is left behind the pulse, at odds with Yoffe's transient opening model. To our knowledge Broberg's work has not been cited in relation with the origin of self-healing rupture pulses, although that developed by Freund (1979) was discussed in Heaton (1990), Perrin *et al.* (1995), and Zheng and Rice (1998). The Freund (1979) model, as emphasized in the study of Perrin *et al.* (1995), requires that frictional strength be recovered rapidly after the onset of healing, a feature also implicitly present in the solution presented here.

While the pulse solution was acknowledged for the steady regime, on an analytical basis, few arguments were made in the framework of self-similarity in favor of or against the uniqueness of the cracklike Kostrov (1964b) solution. In this article we establish that self-healing, self-similar solutions exist at least for 2D antiplane faults, for the same problem as studied by Kostrov. Particular attention is paid to the analysis of singularities, to the stress concentration, and to energetic considerations. Differences and similarities with the Kostrov solution are discussed. We further argue that since the Kostrov solution is not unique, it is possible that an infinity of exotic fracture solutions may exist that satisfy the elastic wave equation, although some may be more likely to develop than others.

We complement our analytical study with a number of numerical simulations in both 2D and 3D, in order to illustrate practically the triggering of the pulselike solution. Once started, it will be maintained even without rate weakening in the friction for 2D cases. However, we note that for 3D elastic cases with elliptical or circular expansion, the healing front is apparently unable to propagate spontaneously into regions with no rate weakening.

The question of the selection of the velocity for the healing front is discussed. Although we have so far been unable to find a theoretical explanation, the numerical examples discussed suggest a lower bound for the the healing front velocity. One difficulty is that in the absence of rate weakening, no controlling dimensionless parameter can be defined, as was done by Zheng and Rice (1998) or by Nielsen and Carlson (2000).

Laplace Transformed Solution to Self-Similar Antiplane Faults

We consider antiplane particle motion in 2D, that is, only the single component $u = u_y$ of displacement is non-zero inside the 2D plane (O, x, z). Let the fault plane lie along the x axis, at $z = 0$. Let the homogenous elastic modulus, density, and shear velocity be μ, ρ and β, respectively. The elastic wave equation in this case reduces to

$$\beta^{-2}\partial_{tt}u(x, z, t) = \partial_{xx}u(x, z, t) + \partial_{zz}u(x, z, t). \quad (1)$$

Let $v(x, t) = \partial_t u(x, t)$ be the y component of particle velocity and $V(x, t)$ be the slip rate between the two sides of the fault, such that $V(x, t) = v(x, 0^+, t) - v(x, 0^-, t)$. Given the symmetry of the problem, v is an odd function of z, so that we can write

$$v(x, 0^+, t) = \frac{1}{2} V(x, t). \quad (2)$$

We shall seek solutions of the wave equation (equation 1) that satisfy the general slip velocity boundary condition (equation 2).

Let us define the double Laplace transform $L_{xt}\{v(x, z, t)\} \rightarrow \tilde{v}(p, s, z)$ as

$$\tilde{v}(p, s, z) = \int_0^\infty dt \int_{-\infty}^{+\infty} dx\, v(x, z, t)\, \mathrm{e}^{-s(t-px)}, \quad (3)$$

with inverse transform:

$$v(x, z, t) = \frac{1}{2\pi i} \int_{C_s} ds \frac{1}{2\pi i} \int_{C_p} dp\, s\, \tilde{v}(p, s, z)\, \mathrm{e}^{+s(t-px)}, \quad (4)$$

where C_s and C_p are appropriate integration contours in the complex plane, also known as Bromwich contours, that we shall define later for our specific case.

We make the assumption that slip velocity V is a general self-similar function, as in the case of the Kostrov crack. Self-similarity of velocity v means that it can be rewritten as a homogeneous function of degree n, $v(x, z, t) = t^n\, v(x/t, z/t)$. In our case, divergence of velocity at $t = \infty$ or at the origin $t = 0$ is unacceptable so that the only possible choice for v is a self-similar function of degree $n = 0$. This also applies to the slip rate V (Fig. 1), which reduces to a function of a single variable, that is,

$$V(x, t) = V(x/t). \quad (5)$$

It can be shown (see Willis [1973]) that the Laplace transform of a self-similar function of order zero can be written as

$$\tilde{V}(p, s) = s^{-2}\tilde{V}(p), \quad (6)$$

where $\tilde{V}$ denotes the Laplace transforms of slip rate [obviously, $\tilde{V}(p, s)$ and $\tilde{V}(p)$ are not the same function, but we retain the same notation for simplicity]. In the Laplace do-

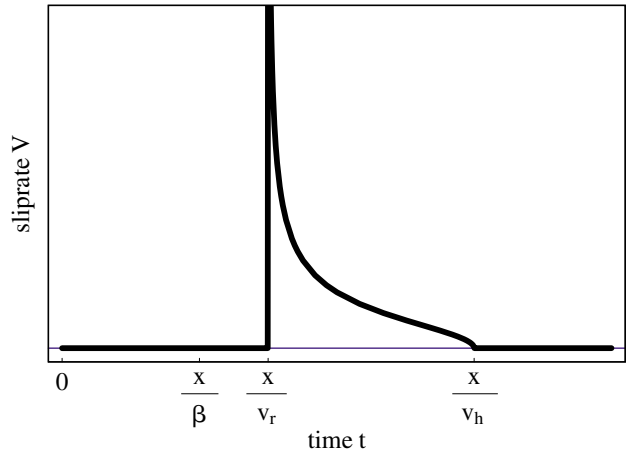

Figure 1. Slip-rate function of t/x, for the unilateral, self-similar pulse. In the example the rupture and healing velocities are $v_r = 2\beta/3$ and $v_h = \beta/3$ [V is normalized by $\mu\beta/(\Delta\sigma)$].

main, solutions of the wave equation (1) with boundary conditions (2) have the general form

$$\tilde{v}(p,\ s,\ z)\ =\ \frac{1}{2}\ \tilde{V}(p,\ s)\ \mathrm{e}^{-sq(p)z}, \tag{7}$$

where the tilde denotes the Laplace transform of particle velocity v and we introduced the vertical slowness $q(p) = \sqrt{1\ -\ p^2}$ (if p is normalized by the shear-wave velocity β; otherwise $q(p) = \sqrt{\beta^{-2}\ -\ p^2}$).

Let us compute now the transform of fault traction $\tilde{\sigma}(p, s, z) = L_{xt}\{\sigma(x, z, t)\}$, where

$$\sigma(x,\ z,\ t)\ =\ \sigma_{yz}(x,\ z,\ t)\ =\ \mu\ \partial_z u(x,\ y,\ z),$$

and let us use the property that derivation with respect to t yields a multiplication by s in the Laplace domain. We get

$$\tilde{\sigma}(p,\ s,\ z)\ =\ \mu s^{-1}\partial_z\tilde{v}(p,\ s,\ z).$$

Upon replacement of $\tilde{v}$ according to equation (7), we obtain

$$\tilde{\sigma}(p,\ s,\ z)\ =\ -\ \frac{\mu}{2}\ q(p)\tilde{V}(p,\ s)\ \mathrm{e}^{-sq(p)z},$$

which on the fault plane reduces to

$$\tilde{\sigma}(p,\ s,\ 0)\ =\ -\ \frac{\mu}{2}\ q(p)\ \tilde{V}(p,\ s). \tag{8}$$

Equation (8) states that fault stress in the Laplace domain is simply the slip rate times $\mu q(p)/2$. We shall take advantage of such a property later, in order to derive the stress field associated to a given form of slip rate. Once the self-similar function (6) is defined, equations (3) and (4) can be used to compute velocities and stresses everywhere in the elastic medium by the Cagniard–de Hoop method.

Kostrov's Self-Similar Crack

Let us begin by recalling some results that were obtained by Kostrov for the self-similar crack. While Kostrov used the methods of Smirnov and Sobolev, we prefer to use the Cagniard–de Hoop technique that is better known in seismology. We start by writing the inverse Laplace transform of slip rate and stress on the fault, according to equations (4), (6), and (8):

$$V(t/x)\ =\ \frac{1}{2\pi i}\int_{C_p} dp\ \frac{1}{2\pi i}\int_{C_s} ds\ s^{-1}\ \tilde{V}(p)\ \mathrm{e}^{-s(t-px)}, \tag{9}$$

$$\sigma(x,\ 0,\ t)\ =\ -\ \frac{1}{2\pi i}\int_{C_p} dp\ \frac{\mu}{4\pi i}\int_{C_s} ds\ s^{-1}\ q(p)\tilde{V}(p)\ \mathrm{e}^{-s(t-px)}. \tag{10}$$

In the case of a crack expanding at constant velocity with a constant stress level imposed inside the actively slipping region, Kostrov (1964b) proposed the following self-similar slip function:

$$\tilde{V}(p)\ =\ \frac{A}{v_r\ (v_r^{-2}\ -\ p^2)^{3/2}}, \tag{11}$$

where A is a constant to be computed, whereas $\nu_r = v_r/\beta$ is the dimensionless rupture velocity and p the dimensionless slowness (in a sense equivalent to $\beta t/x$).

Let us remark that for $V(x/t)$ and $\sigma(x, z, t)$ to be real, the singularities of $\tilde{V}(p)$ must be on the real p line. Furthermore, the exponent of the denominator is not an integer, so that we have a branch point at $p = v_r^{-1}$; another branch point at $p = 1$ comes from the slowness $q(p) = \sqrt{1\ -\ p^2}$ in equation (10). Thus we introduce a branch cut along the real axis, for $1 \le p \le v_r^{-1}$ in the case of equation (10) and for $p \ge v_r^{-1}$ in the case of equation (9). Following Cagniard–de Hoop, the contour C_p is now folded onto the real line above and below the singularity of $\tilde{V}(p)$. Just above the cuts $\mathrm{Im}[q(p)] < 0$ and $\mathrm{Im}[\sqrt{v_r^{-2}\ -\ p^2}] < 0$.

Since p is real on the new contour, the Laplace transform of the Dirac function $\delta(t\ -px)$ is the constant 1, and division by s in the Laplace domain is equivalent to a time integration, we can write by inspection that

$$\frac{1}{2\pi i}\int_{C_s} ds\ s^{-1}\ \mathrm{e}^{-s(t-px)}\ =\ H(t\ -\ px). \tag{12}$$

By noticing that $\tilde{V}(p)$ is imaginary in the domain of interest, we obtain, after replacing equation (12) into equations (9) and (10),

$$V(t/x) = \frac{1}{\pi}\int_0^{t/x} dp\ \mathrm{Im}\ [\tilde{V}(p)], \quad (13)$$

$$\sigma(x, 0, t) = -\frac{\mu}{2\pi}\int_0^{t/x} dp\ \mathrm{Im}\ [q(p)\ \tilde{V}(p)]. \quad (14)$$

These expressions were derived by Kostrov (1964b) with a different technique, essentially by inspection using the Smirnov–Sobolev theory. Integration of equation (13) yields the well-known slip-rate profile:

$$V(x, t) = \frac{A}{\pi}\frac{v_r}{\beta}\,\mathrm{Re}\left[\frac{t/x}{\sqrt{t^2/x^2 - v_r^{-2}}}\right] \quad (15)$$

after substituting $v_r \to v_r/\beta$; $p \to \beta t/x$. Similarly, integration of equation (14) yields stress distribution on the crack, for $v_r > x/t > 1/\beta$:

$$\sigma(x, 0, t) = \frac{A\,\mu}{2\pi\,\beta}\,\mathrm{Re}\left[v_r\frac{t\sqrt{\beta^{-2} - t^2/x^2}}{x\sqrt{t^2/x^2 - v_r^{-2}}}\right] + \frac{A\,\mu}{2\pi\,\beta}\,\mathrm{Im}\left[F\left(\arcsin\frac{\beta t}{x}, \frac{v_r^2}{\beta^2}\right) - E\left(\arcsin\frac{\beta t}{x}, \frac{v_r^2}{\beta^2}\right)\right], \quad (16)$$

where $F(\phi, k)$ and $E(\phi, k)$ are the incomplete elliptical integrals of the first and second kind, respectively (we use the notation proposed in Gradshteyn and Ryzhik [1965]). We remark that for $\beta t > x$, that is, after the arrival of the S wave, $\arcsin \beta t/x$ is purely imaginary.

Inside the crack, for $t/x > v_r^{-1}$, the real part of the first term is zero, while the elliptic integrals yield a constant (see Appendix C). Such a constant corresponds to the stress drop, and we can compute the value of the constant A for a given couple $(\Delta\sigma, v_r)$ by equating equation (16) to the stress drop $\Delta\sigma$:

$$A = 2\pi\,\frac{\beta\Delta\sigma}{\mu}\,\mathrm{Im}\left[F\left\{\arcsin\frac{\beta}{v_r}, \frac{v_r^2}{\beta^2}\right\} - E\left\{\arcsin\frac{\beta}{v_r}, \frac{v_r^2}{\beta^2}\right\}\right]^{-1},$$

where the fault impedance $\mu/2\beta$ has been combined with the dimensionless amplitude term from equation (16). This expression can be simplified using the relation from Appendix C,

$$A = 2\pi\,\beta\,\frac{\Delta\sigma}{\mu}\,\frac{1}{\mathbf{E}(\gamma^2)}, \quad (17)$$

where $\mathbf{E}(\gamma^2)$ is the complete elliptical function of the second kind with $\gamma = \sqrt{1 - v_r^2/\beta^2}$.

Generalization of the Kostrov Solution

The study of the Kostrov solution shows that if one can find any function of p that is real on the real p axis for $p < v_r^{-1}$, this is a legitimate solution to the crack problem. In addition, if one wants to have a finite energy release at the crack front and no additional dislocation sources, we must choose

$$\tilde{V}(p) = \frac{\wp(p)}{(v_r^{-n} - p^{-n})^{3/2}},$$

where $\wp(p)$ is a complex function and $n = 1$ or $n = 2$. In the case of the Kostrov crack, $\wp(p)$ is a constant and $n = 2$, so that the solution is symmetric with respect to $x = 0$. Finite energy release is provided when the the limit of stress in the unbroken vicinity of the fracture tip has the form $r^{-1/2}$, where $r = x - tv_r$ is distance to the crack tip. $\wp(p)$ may have any number of branch cuts along the real axis for $p > v_r^{-1}$. Thus Kostrov's solution is just the simplest of the $\wp(p)$ functions: a constant A. In order to find the appropriate function $\wp(p)$ for a self-healing slip function, we proceed as follows. Upon inspection of numerical simulations, slip-rate functions of self-healing pulses are similar to the singular crack solution at fracture onset, but they appear to be rapidly tapered toward zero near the trailing front where healing occurs. Such features indicate that an expression of $V(x, t)$ for the pulse may be close to that of the self-similar crack, but with an extra term accounting for the trailing edge.

Models of self-healing, propagating rupture pulses of constant width (steady state solution), were presented by Yoffe (1951), Broberg (1978, 1999), and Freund (1979). However, in contrast with previous authors, we seek here solutions of self-similar form, in which a nucleation point and an initial time are defined.

Yoffe's solution described a mode I crack model where the propagating perturbation was opening, then closing again, in such a way so that no net opening was left in the wake of the crack. Such a feature required a stress singularity at both crack ends. However in the solution presented by Freund (1979) for a mode II (shear) crack, the slip velocity never reverses, so that a net displacement is retained in the wake of the healing. Such a feature produces a smooth healing front with no stress singularity, at odds with the mode II solution of Broberg (1978) but in agreement with later works (Broberg, 1999). We note that the fixed width propagating pulse of Freund (1979) and Broberg (1999), $V(x, t) = A\sqrt{(x + h - tv_r)/(tv_r - x)}$, has a square root decay of slip rate toward zero in the trailing edge of the fracture (h is the fixed width of the pulse; $A = v_r\,\Delta\sigma/(\mu\sqrt{1 - v_r^2/\beta^2})$ is a constant amplitude factor). As we will see later, the square root decay is also present in self-similar, self-healing solutions.

We point out that even for self-healing pulses, a finite energy should be absorbed at the rupture front through the development of a stress concentration, in agreement with

classical crack propagation models. However, no energy flow should take place at the healing front, so that we do not expect any stress singularity there.

In prospect, we can anticipate that the solution should have the following properties:

1. A stress singularity of the form $(x - t\,v_r)^{-1/2}$ in the limit close to the crack tip because of the finite energy requirement. This requires the presence of a term in $(p^n - \nu_r^n)^{-3/2}$ in the Fourier transform expression, yielding an inverse square root term once integrated.
2. In practice, only lower powers of p yield solutions of acceptable regularity at the origin. If symmetry with respect to the origin is desired, the function $\wp(p)$ should be even in p. On the other hand, asymmetric solutions with uneven powers of p are not excluded *a priori*, for example, in the case of unilateral propagation.
3. Velocity [$\tilde{V}(p)$ integrated] should taper to zero without discontinuity (in order to meet the energy neutral requirement) at the time of healing; this could be well modeled by a $(\nu_h^{-n} - p^n)^{-1/2}$ term in the polynomial, where $\nu_h = v_h/\beta$ would be the normalized healing front velocity.

On those premises we can propose a function $\wp(p)$ and test whether the boundary conditions in stress are met, following a trial-and-error approach as that of Burridge and Willis (1969), who found the solution for the elliptical, self-similar crack.

The Unilateral Propagating Pulse

We will first discuss the unilateral fracture pulse, the case with most practical implications, both physically meaningful and relatively simple mathematically. In this case, we opt for a Fourier transform where terms in $p^{1/2}$ are involved in such a way that any negative value of p yields a purely imaginary slip rate:

$$\tilde{V}(p) = -A\,\frac{\sqrt{\nu_h}\,(\nu_h{}^{-1} - \nu_r{}^{-1})}{\sqrt{\nu_h{}^{-1} - p}\,(\nu_r{}^{-1} - p)^{3/2}}. \qquad (18)$$

The factor $\sqrt{\nu_h}(\nu_h{}^{-1} - \nu_r{}^{-1})$ was introduced to simplify the resulting velocity expression and to regularize it in the limit $v_h \to 0$. Noting that the new expression for $\tilde{V}(p)$ introduces a new singularity and branch point at $p = \nu_h^{-1}$, after a slight modification of the branch cuts, we remark that an integration contour identical to that of the crack can be applied. Reverse transform of $\tilde{V}(p)$ by Cagniard–de Hoop, following a contour going along the real axis in the upper right quarter plane, yields, after some algebra,

$$V\left(\frac{t}{x}\right) = \frac{A}{\pi}\sqrt{\frac{v_r}{\beta}}\,\frac{\sqrt{x - t\,v_h}}{\sqrt{t\,v_r - x}}, \qquad (19)$$

where we have reintroduced the scaling with respect to shear-wave speed β by substituting

$$\nu_r \to v_r/\beta,$$
$$\nu_h \to v_h/\beta,$$
$$p \to \beta t/x.$$

As usual, the amplitude term A scaling slip rate to the stress drop is to be evaluated once the stress value is derived in quite the same way as for the Kostrov crack (equation 17); note that in our definition A has the dimensions of a velocity. An example of the resulting curve is represented in equation (19).

By construction this slip-rate function is self-similar; it tapers to zero when $x \to v_h$ from above, it is singular when $x \to t\,v_r$ from below, and it is zero both before fracture and after healing. Near the rupture front as $x \to t\,v_r$, $\tilde{V}(t/x)$ behaves just like the Kostrov slip-rate function (equation 15). Indeed, we show further that in the region just behind the rupture front, we obtain the same limit.

We can now verify that stress drop is constant inside the actively slipping region, in agreement with the boundary conditions prescribed. Introducing transform (18) into equation (14), after integration and some algebra, a closed expression for the stress can be obtained as a sum of several terms including elliptic integrals, that is, the real part of

$$\begin{aligned}\sigma\left(\frac{t}{x}\right) = \frac{A\mu}{2\pi\beta}\,\mathrm{Re}\Bigg(&\left(2 - 2\sqrt{\frac{\beta}{v_r}}\right)\sqrt{\frac{x+t\beta}{x-t\beta}}\,\sqrt{\frac{tv_h - x}{x - tv_r}} \\ &+ 4\,\frac{\left(1 - \frac{v_h}{v_r}\right)\sqrt{\beta v_r}}{\sqrt{(\beta + v_h)(\beta - v_r)}}\left\{F\left(\arcsin\left(\sqrt{\frac{x+t\beta}{t\beta - x}}\,\sqrt{\lambda}\right), \frac{\zeta}{\lambda}\right)\right. \\ &\left. - \Pi\left(\frac{1}{\lambda}, \arcsin\left(\sqrt{\frac{x+t\beta}{t\beta - x}}\,\sqrt{\lambda}\right), \frac{\zeta}{\lambda}\right)\right\} \\ &+ 2\sqrt{\frac{(\beta + v_h)(\beta - v_r)}{\beta\,v_r}}\,E\left(\arcsin\left(\sqrt{\frac{x+t\beta}{t\beta - x}}\,\sqrt{\lambda}\right), \frac{\zeta}{\lambda}\right)\Bigg),\end{aligned} \qquad (20)$$

$$\text{where } \lambda = \frac{\beta - v_r}{\beta + v_r},\ \zeta = \frac{\beta - v_h}{\beta + v_h},$$

and F, E, and Π refer to elliptic integrals of the first, second, and third kind, respectively (see Appendix C). This function is plotted in Figure 2 as a function of time and in Figure 3 as a function of x.

We remark that the stress effectively drops to a constant value, which can be chosen as the zero reference state, in the actively sliding area $v_h < x/t < v_r$, for all variable terms become purely imaginary in that interval. Before the arrival of waves ($t < x/\beta$), too, all terms become imaginary except for the integral terms, which reduce to constant, complete

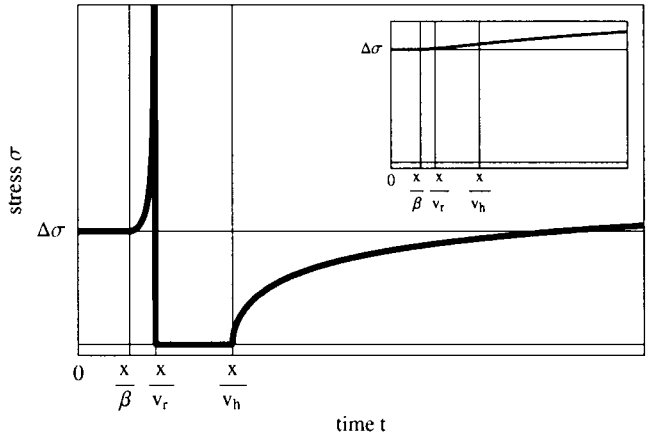

Figure 2. Stress as a function of t/x, for the unilateral, self-similar pulse. In the example the rupture and healing velocities are $v_r = 2\beta/3$ and $v_h = \beta/3$. Note that on the healed portion, the stress continuously increases, as long as the pulse continues to propagate, eventually reaching and surpassing the initial level. The persistence of such an increase toward the limit $t/x \to \infty$ corresponds to a stress singularity located at $x = 0$, represented in Figure 3. The incerpt represents the stress trend on a point along the negative x axis (unbroken side), with an increase slowly starting at the arrival of the first shear waves from the nucleation point.

elliptic integrals. The difference between stress in the two intervals corresponds to the constant stress drop inside the faulted zone, so that by equating it to $\Delta\sigma$, it is possible to obtain the normalized amplitude A in the form

$$A = 2\pi \frac{\beta\Delta\sigma}{\mu}\left(4\frac{\left(1-\frac{v_h}{v_r}\right)\sqrt{\beta\, v_r}}{\sqrt{(\beta+v_h)\,(\beta-v_r)}}\left(\mathbf{F}\left(\frac{\zeta}{\lambda}\right)-\mathbf{\Pi}\left(\frac{1}{\lambda},\frac{\zeta}{\lambda}\right)\right)+2\sqrt{\frac{(\beta+v_h)\,(\beta-v_r)}{\beta v_r}}\,\mathbf{E}\left(\frac{\zeta}{\lambda}\right)\right). \quad (21)$$

The **E**, **F**, and **Π** functions now represent complete elliptic integrals.

The stress expression has two remarkable features. First, the singularity right before rupture yields the correct behavior in $1/\sqrt{x - tv_r}$; second, there is also a singularity at the origin (in the limit $x/t \to 0$). Such a feature is due to the nonsymmetry of the unilateral propagation. In the limit where the healing front does not propagate, the singularity at the origin corresponds to the arrested edge of a unilateral propagating crack. In the case of a propagating healing front, on the other hand, it is linked to the sudden rupture in the slope of the slip function at $x = 0$. Upon reflection, it is obvious that the unbroken semiaxis ($x < 0$) remains at zero slip on its whole length, while in the healed portion of the broken side ($0 < x < tv_r$) we expect a constant, positive slope, as a direct consequence of self-similarity and a rise time proportional to position.

This is confirmed indeed if we compute the slip function by simple integration of $V(x, t)$ with respect to t, assuming a fixed x, to retain the real part of

$$u(x,\,t) = 2\frac{A}{\pi}\sqrt{\frac{v_r}{\beta}}\frac{\sqrt{tv_r - x}\,\sqrt{x - tv_h}}{v_r} - 2\frac{A}{\pi}\sqrt{\frac{v_r}{\beta}}\frac{(v_r - v_h)\,x}{2v_r\sqrt{v_h\,v_r}}\left(\arctan\left[\frac{-2t\,v_h\,v_r + x(v_r + v_h)}{2\sqrt{t\,v_r - x}\,\sqrt{x - t\,v_h}\,\sqrt{v_h\,v_r}}\right] - \frac{\pi}{2}\right), \quad (22)$$

which is illustrated in Figure 3. Slip shows the expected, intuitive linear dependence in x: since the pulse width is zero at the origin and expands linearly with x, the slip that it leaves in its wake should also increase linearly with x. Moreover, it is obvious that slip remains constant at a given position x after healing. There is a striking feature of the slip, inside the active area, when represented as a function of position: one would expect that it reaches a maximum at the queue of the pulse, right next to the healing front. On the contrary, it does not decrease monotonously as a function of position, but reverses slope slightly above $t\,v_h$, which is surprising at first sight. However, this representation does not imply that slip rate becomes negative at any time. Indeed we have, at any given time, a series of points at different stages of evolution inside the pulse. The slope inversion shortly above $t\,v_h$ is in fact due to the shorter pulse duration for inner points. Slip as a function of time, position fixed, shows a simpler, monotonously increasing trend from rupture time until it reaches its maximum value, then heals (Fig. 4).

The slip-rate solution is strikingly similar to that for the propagating pulse of fixed width h, $V(x, t) = A\sqrt{(x + h - t\,v_r)/(t\,v_r - x)}$ (Broberg, 1978, 1999; Freund, 1979). In fact the two solutions are exactly superimposable, at any fixed time t, by substituting $t(v_r - v_h) \to h$. Further, we can point out that the steady state solution is a self-similar solution in the limit where healing and rupture fronts become parallel, that is, $v_h \to v_r$.

In synthesis, we have found a self-healing, self-similar solution with classical boundary conditions; the resulting velocity, stress, and displacement functions are represented in Figure 3 as a function of position, at an arbitrary given time t, for the case $v_r = 2/3\beta$, $v_h = 1/3\beta$.

In Appendices A and B we propose two more solutions, the bilateral pulse and the antisymmetric pulse, essentially as curiosities of limited practical interest, but also as useful illustrations of the potential existence of many more solutions.

Properties in the Vicinity of Fracture Front

We can determine now the behavior of our solutions near the rupture front when $t \to x/v_r$. As we explained earlier,

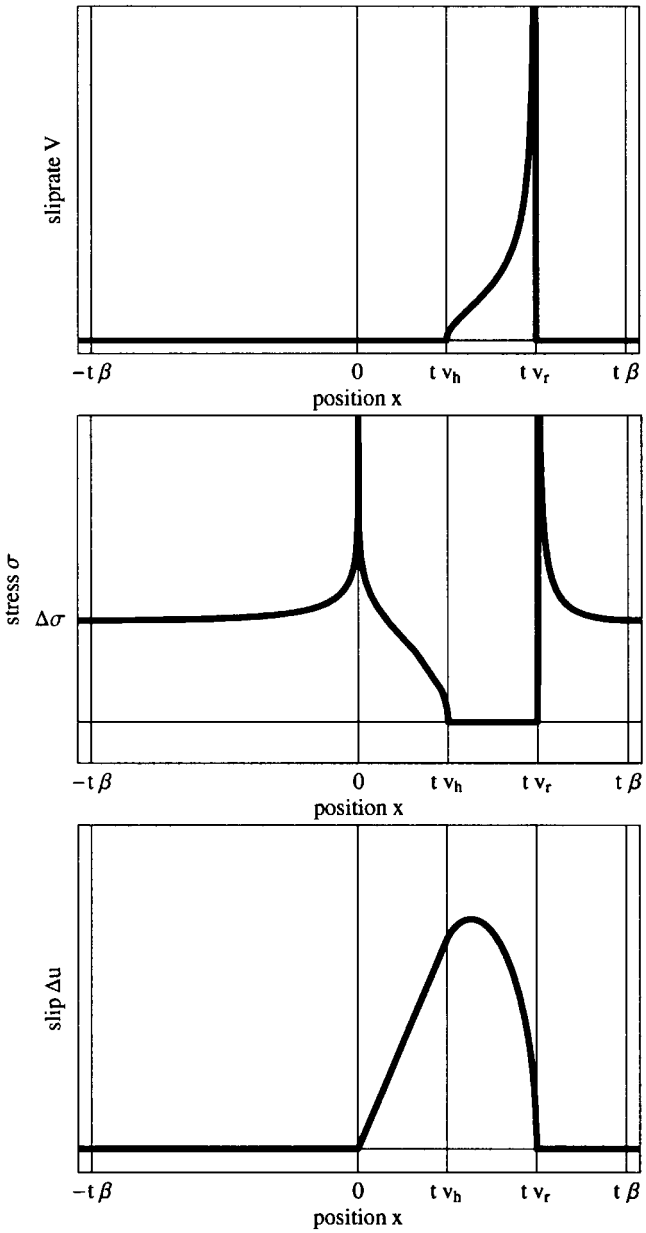

Figure 3. Slip rate (top), stress (middle), and slip (bottom) as a function of position, at fixed time t (same normalization and velocity parameters as in Fig. 1). See text for further details.

we normalized the slip-rate functions such that they had the same behavior near the rupture front. We find from equation (19) that the slip-rate field behaves like

$$\lim_{x\uparrow v_r t} V(x/t) = \frac{2A}{\pi}\sqrt{\frac{v_r}{\beta} - \frac{v_h}{\beta}}\,\frac{\sqrt{v_r\, t}}{\sqrt{v_r\, t - x}}.$$

Similarly, just ahead of the rupture front the stress field is, from the singular terms in equation (20),

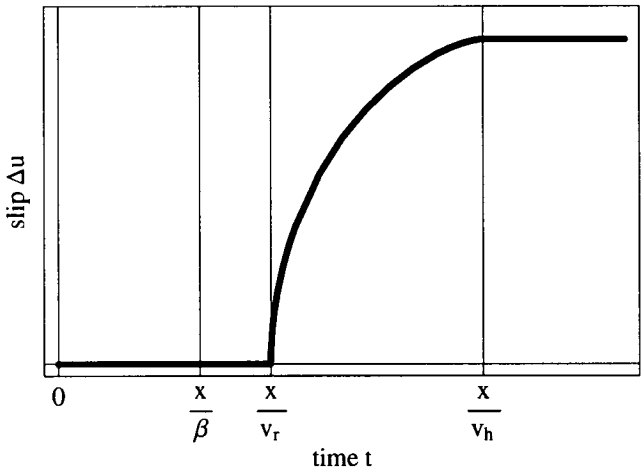

Figure 4. Slip as a function of time (top). The time axis and the slip both scale with the position of the fixed observation point x. In this figure, slip is intended as twice the displacement, that is, $U = u|_{z=0+} - u|_{z=0-}$.

$$\lim_{x\downarrow v_r t} \sigma(x,\, 0,\, t) = \frac{\mu A}{\beta\pi}\sqrt{\frac{v_r}{\beta} - \frac{v_h}{\beta}}\sqrt{1 - \frac{v_r^2}{\beta^2}}\,\frac{\sqrt{tv_r}}{\sqrt{x - tv_r}},$$

which is the same as that for the crack, except for the multiplying constant terms. In the following we will assume that the stress drop is the same in the freely slipping areas and we will refer all our results to stress drop. The stress outside the crack is given by the singular terms in the expressions for stress. We write the stress singularity in the usual notation,

$$\sigma(x,\, 0,\, t) = \frac{1}{\sqrt{2\pi}}\, K_{\mathrm{III}}\,\frac{1}{\sqrt{x - v_r t}},$$

where K_{III} is the stress intensity factor for mode III, antiplane shear. For the Kostrov model we get from equation (16)

$$K_{\mathrm{III}} = \sqrt{\pi}\,\Delta\sigma\sqrt{v_r t}\,\frac{\gamma}{\mathbf{E}(\gamma^2)},$$

where $\mathbf{E}$ is the complete elliptical integral of argument γ^2, where

$$\gamma = \sqrt{1 - v_r^2/\beta^2}.$$

This result is in full agreement with the result of Broberg (1999). For the self-healing pulse we get from equation (20)

$$K_{\mathrm{III}} = 2A\sqrt{2\pi}\sqrt{\frac{\beta}{v_r}}\sqrt{1 - \frac{v_h}{v_r}}\,\sqrt{v_r t}\gamma,$$

where A is given by equation (21).

Finally we can compute the energy flow into the rupture front, using the standard definition (Broberg, 1999):

$$\mathcal{G} = \frac{K_{\mathrm{III}}^2}{2\mu}\,\frac{1}{\gamma}.$$

Although not obvious from these expressions, the K_{III} and $\mathcal{G}$ expressions for the crack and the pulse share great similarities; in particular, when the rupture velocity approaches the shear-wave speed, they converge toward the same limit, as illustrated graphically (Fig. 5). Furthermore, at vanishing small rupture velocity, the case $v_{\mathrm{h}} = 0$ has exactly half the energy flow of a crack; indeed this situation corresponds to two quasi-static cracks, where one is twice as large as the other.

For the same stress drop $\Delta\sigma$ in the broken area between the rupture and the healing front, and for the same rupture speed v_{r}, the energy release rate decreases as v_{h} increases. Figure 5 compares the behavior of the energy release rate $\mathcal{G}$ at four different healing rates with the energy flow for Kostrov's solution (dotted line). This figure illustrates a fundamental difference between crack and pulselike ruptures: indeed, in the latter case $\mathcal{G}$ does not decrease monotonously with rupture velocity v_{r}. There is a critical limit below which energy flux decreases as the rupture slows down, so that the rupture process will become unstable and rapidly stop as soon as velocity falls below such limit. The opposite occurs in the case of the crack, where rupture slowness is always compensated by an increase in the energy flux (note that the same observation holds for the behavior of stress concentration K_{III}). This explains why it is much easier to stop rupture pulses than cracks.

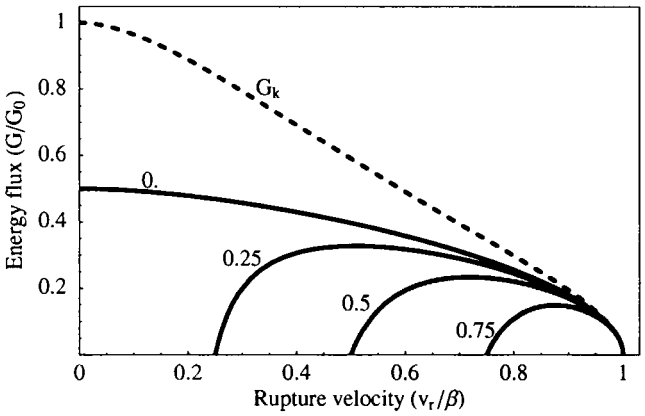

Figure 5. Energy flux $\mathcal{G}$ at the crack tip as a function of rupture velocity v_{r}. The dotted curve $\mathcal{G}_{\mathrm{k}}$ represents the case of the Kostrov crack (no healing); the solid curves represent self-healing pulses at four different healing rates ($v_{\mathrm{h}} = 0v_{\mathrm{r}}$, $0.25v_{\mathrm{r}}$, $0.5v_{\mathrm{r}}$, and $0.75v_{\mathrm{r}}$). Note that all solutions converge in the limit $v_{\mathrm{r}} \to \beta$: this means that when the fracture is propagating fast, the tip does not see what happens backward, so that in the limit $v_{\mathrm{r}} \to \beta$ all models are equivalent. Moreover, note that when v_{h} and v_{r} coincide, the energy flux vanishes, as a direct consequence of the slipping area tending to zero, with the obvious exception of $v_{\mathrm{h}} = 0$. In the case of a pulse, the energy flux does not decrease monotonously with rupture velocity; this feature explains why it is much easier to stop a pulse than a crack (see text for further explanations). All $\mathcal{G}$ values are normalized by the value $\mathcal{G}_0 = \lim_{v_{\mathrm{r}}\uparrow 0i} \mathcal{G}_{\mathrm{k}}$, that is, the energy flux for the crack at negligible rupture velocity.

Behavior at the Healing Front

We can now study in some detail the behavior of slip rate and stress near the healing front as $v_{\mathrm{h}}t$ approaches x. For the slip rate we get

$$\lim_{x\uparrow v_{\mathrm{h}}t} V(x,\,t) = \frac{2A}{\pi}\sqrt{\frac{v_{\mathrm{h}}}{\beta} - \frac{v_{\mathrm{r}}}{\beta}}\,\frac{\sqrt{x - t\,v_{\mathrm{h}}}}{\sqrt{v_{\mathrm{h}}\,t}} \qquad (23)$$

and for the stress

$$\lim_{x\downarrow v_{\mathrm{h}}t} \sigma(x,\,0,\,t) = \frac{\mu A}{\beta\pi}\sqrt{1 - \frac{\beta^2}{v_{\mathrm{h}}^2}}\,\sqrt{\frac{v_{\mathrm{r}}}{\beta} - \frac{v_{\mathrm{h}}}{\beta}}\,\frac{\sqrt{x - t\,v_{\mathrm{h}}}}{\sqrt{v_{\mathrm{h}}t}}, \qquad (24)$$

and we recall that A is defined in equation (21).

Thus both the slip rate and stress change have matching square-root singularities. No energy is dissipated by healing, in the sense that there is no energy flow through the end of rupture; in our model once healing starts, it propagates without any further dissipation. However the very presence of healing affects the energy flow at the fracture tip by modifying the overall slip solution.

Behavior at the Origin and Refracturing

By setting $v_{\mathrm{h}} = 0$, the solution becomes a unliateral propagating crack and the stress peak at $x \to 0^-$ becomes the usual stress singularity at the crack edge. Alternatively, if the healing front propagates ($v_{\mathrm{h}} > 0$) it can be shown that the stress peak at the origin (see Fig. 3) forms a logarithmic singularity in the limit $x/t \to 0$. What are then its practical implications?

In more complex, realistic models in the presence of a slip-weakening mechanism, all singularities will be blunted, but nonetheless they appear in the theoretical limit where the slip-weakening region becomes infinitesimal with respect to the length of the continuously propagating crack (or pulse). Thus, even in blunt models, there will be an initially moderate stress concentration at the origin that will tend to grow sharper in time as the pulse continues to propagate and expand self-similarly. In the case of a continued propagation, stress at the origin will eventually reach any given threshold. A second fracture is then likely to nucleate and start to propagate, in the form of a second, inner pulse. The latter may

soon die out, when encountering lower stress regions, or continue to develop to some extent. This feature, which we may describe as a refracturing process, has already been observed in at least two numerical studies of dynamic fracture in the presence of self-healing pulses (see figure 4 in Nielsen *et al.* [2000] and also examples in Cochard and Madariaga [1996]).

If the reader finds the mechanism counterintuitive, it can nonteheless be understood with the help of a simple mind experiment. Let an earthquake A propagate over an asperity S_a of a fault and stop. Let then an earthquake B affect the same fault but on a neighboring region S_b, initially not overlapping S_a. If earthquake B is sufficiently large and/or close to area S_a, it may trigger again fracture inside S_a or simply propagate inside it. Let now the time delay between the two earthquakes be so small that they behave altogether as a fracture sequence of two asperities belonging to the same event. Finally, if we let the healing process of A and the triggering of B happen in a smooth transition, the whole process can be viewed as a rupture pulse propagating, followed by refracturing.

Selection of Pulselike Solutions: Numerical Examples

We shall now illustrate the triggering and propagation of the healing front with numerical examples. In particular, we show how the healing front, triggered at fracture onset, propagates persistently even into regions with no rate weakening for 2D, antiplane (mode III) cases. We show that, surprisingly, we obtain a different behavior for the 3D elastic or acoustic cases, with circular or elliptical propagation, where the healing front stops in regions without rate weakening. All simulations are done, for simplicity, with parameters $\mu = \beta = \rho = 1$ (and $\alpha = \sqrt{3}\beta$ for 3D elastic cases). The numerical method of solution was presented in Nielsen and Carlson (2000); the reader is referred to that article for further details on the numerical method.

2D Antiplane Numerical Examples

We start by showing one example of persistent healing front propagation. Rupture was initiated by imposing fracture inside an initial asperity of half-length $x_i = 30\,dx$, where $dx = 0.5$ is the sampling space of the finite difference grid. Rate-weakening friction was imposed only within the initial asperity, in order to trigger self-healing easily, with a characteristic rate $V_c = 2.5$. On the remainder of the fault ($|x| > x_i$) no rate weakening was present. The singularity at the rupture front was regularized, as usual, by introducing a moderate slip weakening with characteristic distance $D_c = 2$. Prestress and yield stress were set to 0.8 and 1.0, respectively. As seen in Figure 6, the rupture front rapidly approaches the shear-wave velocity β, which is the asymptotic limit at $t \to \infty$. On the other hand, the healing front triggered at the onset penetrates regions with no rate weakening ($x > x_i$) and gradually accelerates until it reaches a constant velocity of $v_h \simeq 0.35\, v_r$. Obviously, in this example both rupture triggering and friction are different from the analytical self-similar model; moreover, rupture and healing are allowed to occur spontaneously. As a result, there is a slightly more complex initial transient and no infinite velocity or stress peak at the rupture front. With those premises, Figure

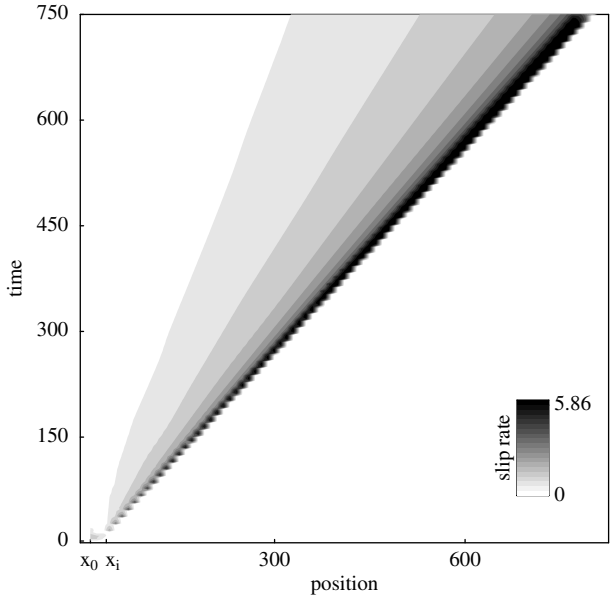

Figure 6. Slip rate in time and space, from a numerical example of spontaneously propagating slip pulse. Healing is initiated by imposing a slight rate weakening in the initial asperity only ($x_0 < x < x_i$). For $x > x_i$ (away from the initial asperity) no rate weakening is present, but the healing front generated at start off is now self-sustained. Healing progressively accelerates and spontaneously sets to a stable value $v_h \simeq 0.35\, v_r$ at $t \simeq 150$.

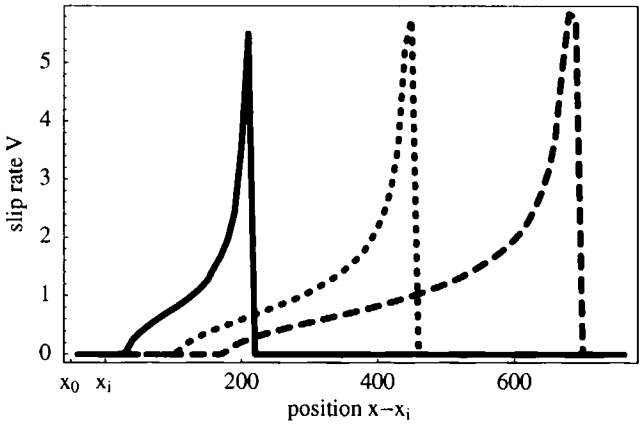

Figure 7. Slip-rate curves from a numerical example of spontaneously propagating slip pulse. The three curves correspond to $t = 230$ (continuous curve), $t = 470$ (thin dashed curve), and $t = 700$ (loosely dashed curve). Position is read with respect to the site x_i of the initial asperity tip ($x_i = 30$).

7 shows slip-rate curves almost identical, by inspection, to the analytical result illustrated in Figure 3, and self-similarity appears by comparing the curves at three different time steps. Such a spontaneous convergence toward a stable, self-similar form after an initial transient was shown in more detail by Nielsen and Carlson (2000).

The Question of the Healing Front Speed

In principle, the solution that we described applies to any case where $0 < v_h < v_r < \beta$, with no *a priori* restriction or preferred value for the healing velocity. In mode III, under homogeneous conditions, rupture speed v_r generally increases approaching asymptotically the shear-wave speed. In mode II, the question is more complex, but admissible final, stable velocities are found theoretically and experimentally in the sub-Rayleigh range or in the intersonic range between shear and tension wave velocities (e.g., see Rosakis *et al.*, 2000). Stability of rupture velocity in crack solutions has classically been investigated through energy considerations, by assuming that there is a positive flux into the rupture tip (Burridge, 1973). For our new self-healing rupture pulse, the same analysis is valid for the rupture front because, as shown in the section on fracture energy, the pulses have the same asymptotic behavior near the rupture front as Kostrov's crack. That is indeed a systematic observation in the numerical experiments both here and in Nielsen and Carlson (2000).

As far as the healing front is concerned, on the other hand, no simple energy consideration is available for selecting admissible values of the healing speed v_h because the energy flow is zero at the healing front since there is no stress or slip-rate singularity associated with healing. We do not know why the healing front should propagate at one rather than another velocity. It is clear from the simulations, however, that a very stable velocity is selected, independently of initial stress conditions, of the order of $v_r = 0.35\beta$, in those regions where no rate weakening is present (Fig. 8). This value coincides with the lowest healing rates found by Nielsen and Carlson (2000) at low levels of rate weakening. Indeed, they were able to obtain higher healing rates at higher levels of rate weakening, but, while the weakening was reduced, the range $0 < v_h < 0.35\ v_r$ seemed to remain excluded. While dimensional arguments are available that indicate a faster healing at higher weakening rates, no such dimensional argument exists in the absence of rate weakening. From experiments both with and without weakening, it seems that $v_r \simeq 0.35$ is a lower limit for admissible healing velocity, although we found no theoretical justification for this result.

It is important to notice that the healing front described here is subshear, so that stresses and velocities at the healing front (equations 23 and 24) are Hilbert conjugate functions. Actually, the local stress and velocity discontinuities at the healing front can be derived from each other using the equations in Ida (1972). On the other hand, for simple velocity weakening friction as studied by Cochard and Madariaga (1994), the healing front is always supershear. Only at supershear speeds can the particle velocity and shear stress have the same kind of discontinuity after the passage of the healing front. No such solution is possible in our problem, because the healing front must be slower than the rupture front for a self-similar solution to the antiplane crack problem to exist.

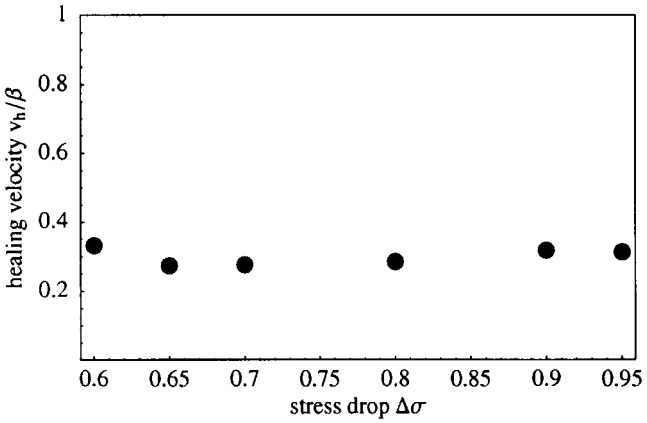

Figure 8. Invariance of v_h with stress drop, in the absence of rate weakening. We think that the small fluctuations about 0.35 are not important and attribute them to a lack of accuracy in estimation of healing speed over the finite time interval of the simulations.

3D Examples

We did simulations for several different 3D models, including (1) 3D acoustic models with cylindrical symmetry and circular fracture, reproducing the model described by Nielsen and Carlson (2000), and (2) fully elastic, homogeneous models where fracture was spontaneously developing either within an elliptical front or, in some cases, within a slightly more complex shape, due to the formation of supershear transition lobes along the slip direction. In none of the instances were we able to observe a persisting healing front in those regions of the fault where no rate weakening was present (see Fig. 9 and 10). These results are strongly at odds with those obtained in all the 2D simulations. However, the healing front was observed to propagate persistently for most cases where the rate weakening was maintained, in agreement with Nielsen and Carlson (2000), as seen in Figure 11.

Conclusions and Perspectives: Exotic Solutions

We have established that self-healing cracklike solutions exist in a strictly antiplane self-similar problem with simple Coulomb friction. Broberg (1978) and Freund (1979) had shown earlier that self-healing solutions also existed for fixed width pulses, so that it may not be necessary to invoke complex friction laws or heterogeneities to explain the evidence of self-healing rupture pulses in a number of observations and numerical simulations. The only problem is to initiate them, but as shown here a moderate amount of velocity weakening or heterogeneity can start a self-healing

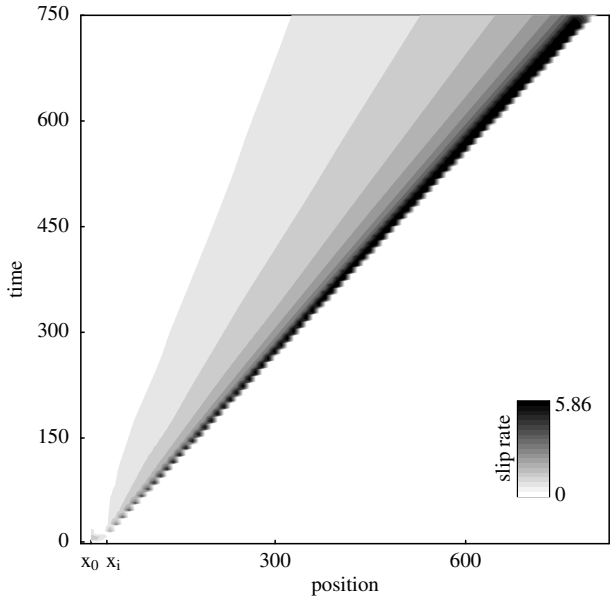

Figure 9. Simulation of self-healing in a 3D, acoustic medium with circular symmetry. In this case we find that the healing front rapidly stalls after entering the region with no rate weakening ($x > x_i$). Compare with the 2D case of Figure 6.

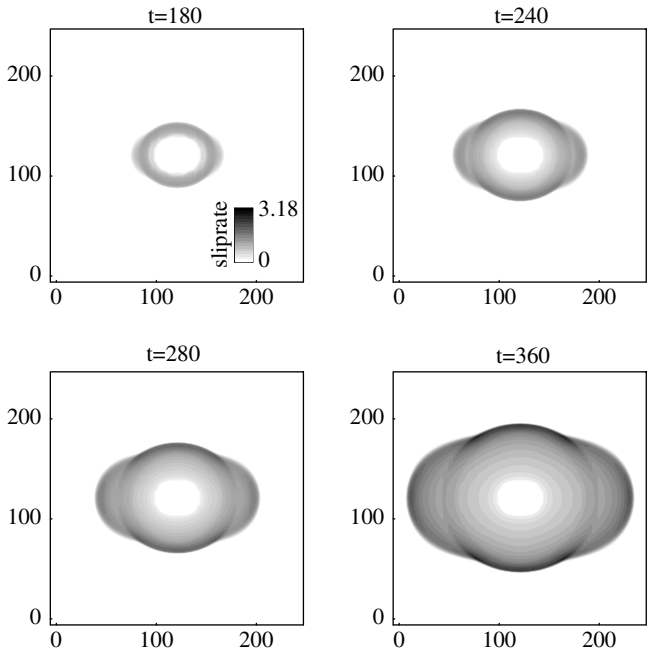

Figure 10. This illustrates the behavior of a fully 3D elastic model, with snapshots of slip rate on the fault at four successive times. The central elliptical region with zero slip rate has healed, due to the presence of rate weakening. However, healing does not propagate to the outer regions of the fault where no rate weakening is present. The side lobes are due to rupture transition to supershear velocity.

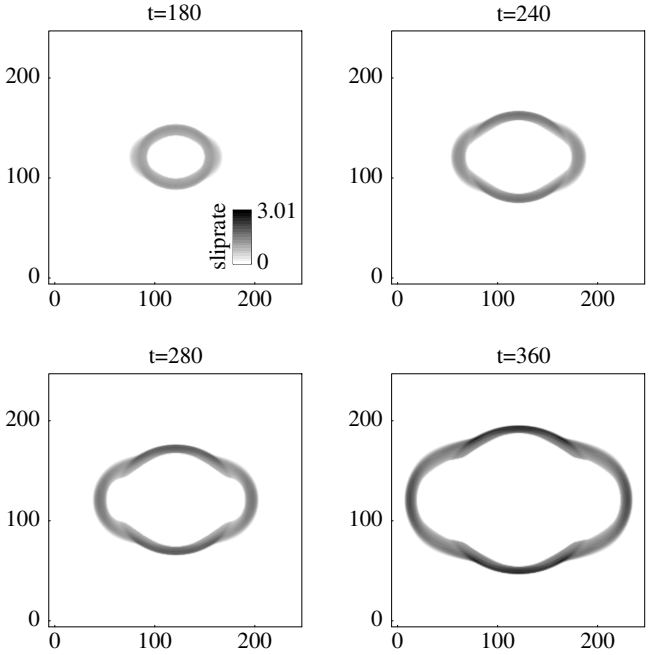

Figure 11. Same model as Figure 10, but in this case the rate weakening was extended to the entire fault. The healing front propagates persistently, spontaneously adopting a profile that matches the rupture front, and the solution appears to be stable.

pulse that will then propagate persistently. For instance, the series of rupture pulses shown in figure 13 of Cochard and Madariaga (1996) may be self-sustained in a crack with classical friction law, although in Cochard and Madariaga (1996) they were computed with a slip-rate-dependent friction law.

The most important result of this work, beyond the particular solution proposed, is a clear illustration that the Kostrov self-similar crack solution is not unique. Any fracture form satisfying both the requirement of finite energy in the limit $t \to x/v_r$ (i.e., close to the crack tip) and the boundary conditions (i.e., stress relief inside the active fracture) will yield a persistent self-similar solution. The implication is that, in addition to the Kostrov crack and the self-healing pulse studied here, there may be other marginally stable, yet unknown, fracture modes that could spontaneously develop depending on the conditions of fracture triggering.

It may however be possible, although not demonstrated, that only the expanding crack solution with no self-healing allows stress to be bounded everywhere away form the fracture fronts, among self-similar models. The solutions found here (with the exception of the pulse propagating away from a rigid body presented in Appendix B) all develop stress singularities at the nucleation site. In the special case of a zero healing velocity (or unilateral crack), the nucleation singularity simply becomes the stress concentration at the fixed fracture edge. As discussed in the Behavior at the Origin and Refracturing section, we do not dismiss as unrealistic the stress singularity at the site of nucleation any more than a

stress singularity at the rupture edge, in the sense that the sharp crack solution is to be considered as a limit.

Further intriguing questions and developments are suggested by this study. The 2D plane problem needs to be analyzed, although it is very likely that a self-healing pulse solution exists in that case for the same velocity function (equation 18) and a somewhat different stress field. The 3D solution for the circular or elliptical self-similar pulse, equivalent to this 2D case, needs also to be analyzed. Although work in that direction is in progress, no complete solution has been reached yet due to the increased complexity of 3D Cagniard–de Hoop (see Willis [1973] for a general theory of 3D elastic waves). Second, the question of the apparently stable healing front velocity systematically selected in the 2D simulations in the absence of rate weakening is still unexplained at the moment. Third, why does the healing front stop in regions with no rate weakening for 3D cases, while it persistently propagates in equivalent 2D cases? An obvious answer, to be investigated, is that the healing front is unstable in 3D because of the combined effects of plane and antiplane modes of rupture and healing. It may be that the healing front undergoes geometrical attenuation in 3D so that it becomes too weak to sustain itself persistently unless a minimum rate-weakening amount is present. Such minimum amount could also be estimated using, for example, a numerical approach similar to that adopted in Cochard and Rice (1997) or Nielsen and Carlson (2000).

Acknowledgments

We thank Jim Rice for his very helpful review of the original version of this article, indicating a parity error that had eluded us. Partial support of this work was provided by the Italian GNDT-INGV framework program 2000–2003 and by the French Minister of Research under ACI Catastrophes Naturelles. S.N. acknowledges the support of the Dipartimento di Scienze Fisiche, Università di Napoli Federico II, currently hosting him.

References

Anoshehpoor, A., and J. Brune (1999). Wrinkle-like Weertman pulse at the interface between two blocks of foam rubber with different velocities, *Geophys. Res. Lett.* **23,** 2025–2028.

Baumberger, T., C. Caroli, and O. Ronsin (2002). Self-healing slip pulses along a gel/glass interface, *Phys. Rev. Lett.* **88,** 075509.

Ben-Zion, Y., and D. J. Andrews (1998). Properties and implications of dynamic rupture along a material interface, *Bull. Seism. Soc. Am.* **88,** 1085–1094.

Beroza, G., and T. Mikumo (1996). Short slip duration in dynamic rupture in the presence of heterogeneous fault properties, *J. Geophys. Res.* **101,** 22,449–22,460.

Broberg, K. (1978). On transient sliding motion, *Geophys. J. R. Astr. Soc.* **52,** 397–432.

Broberg, K. B. (1999). *Cracks and Fracture*, Academic, New York.

Burridge, R. (1973). Admissible speeds for plane-strain self-similar shear cracks with friction but lacking cohesion, *Geophys. J. R. Astr. Soc.* **35,** 439–455.

Burridge, R., and J. R. Willis (1969). The self-similar problem of the expanding elliptical crack in an anisotropic solid, *Proc. Cambridge Phil. Soc.* **66,** 443–468.

Cochard, A., and R. Madariaga (1994). Dynamic faulting under rate-dependent friction, *Pure Appl. Geol. Phys.* **142,** 419–445.

Cochard, A., and R. Madariaga (1996). Complexity of seismicity due to highly rate-dependent friction, *J. Geophys. Res.* **101,** 25,321–25,336.

Cochard, A., and J. Rice (1997). Mode of rupture, self-healing pulse versus enlarging shear crack, for a velocity weakening fault in a 3D solid (abstract), *EOS* **78** (Fall Meeting Suppl.), F472.

Cochard, A., and J. Rice (2000). Fault rupture between dissimilar materials: ill-posedness, regularization, and slip-pulse response, *J. Geophys. Res.* **105,** no. 11, 25,891–25,907.

Day, S. M. (1982). Three-dimensional finite difference simulation of fault dynamics: rectangular faults with fixed rupture velocity, *Bull. Seism. Soc. Am.* **72,** 705–727.

Freund, L. B. (1979). The mechanics of dynamic shear crack propagation, *J. Geophys. Res.* **84,** 2199–2209.

Gradshteyn, I., and I. M. Ryzhik (1965). *Table of Integrals, Series, and Products*, Academic Press, New York.

Heaton, T. H. (1990). Evidence for and implications of self-healing pulses of slip in earthquake rupture, *Phys. Earth Planet. Interiors* **64,** 1–20.

Ida, Y. (1972). Cohesive force across the tip of a longitudinal-shear crack and Griffith's specific surface energy, *J. Geophys. Res.* **77,** 3796–3805.

Johnson, E. (1990). On the initiation of unidirectional slip, *Geophys. J. Int.* **101,** 125–132.

Johnson, E. (1992). The influence of the lithospheric thickness on bilateral slip, *Geophys. J. Int.* **108,** 151–160.

Kostrov, B. (1964a). Self-similar problems of propagation of shear cracks, *Applied Math. Mech.* **28,** 889–898.

Kostrov, B. V. (1964b). Self-similar problems of propagation of shear cracks, *J. App. Math. Mech.* **28,** 1077–1087.

Madariaga, R., and A. Cochard (1994). Seimic source dynamics, heterogeneity, and friction, *Ann. Geofis.* **37,** 1349–1375.

Nielsen, S. B., and J. M. Carlson (2000). Rupture pulse characterization: self-healing, self-similar, expanding solutions in a continuum model of fault dynamics, *Bull. Seism. Soc. Am.* **90,** 1480–1497.

Nielsen, S. B., J. M. Carlson, and K. B. Olsen (2000). Influence of friction and fault geoetry on earthquake rupture, *J. Geophys. Res.* **105,** 6069–6088.

Perrin, G. O., J. R. Rice, and G. Zheng (1995). Self-healing slip pulse on a frictional surface, *J. Mech. Phys. Solids* **43,** 1461–1495.

Rosakis, A. J., O. Samudrala, and D. Coker (2000). Intersonic shear crack growth along weak planes, *Mat. Res. Innovat.* **3,** 236–243.

Rubio, M., and J. Galeano (1994). Stick-slip dynamics in the relaxation of stresses in a continuous elastic medium, *Phys. Rev. E* **50,** 1000–1004.

Weertman, J. (1980). Unstable slippage across a fault that separates elastic media of different elastic constants, *J. Geophys. Res.* **85,** 1455–1461.

Willis, J. R. (1973). Self-similar problems in elastodynamics, *Phil. Trans. R. Soc.* **274,** 435–491.

Yoffe, E. (1951). The moving Griffith crack, *Phil. Mag.* **42,** 739–750.

Zheng, G., and J. Rice (1998). Conditions under which velocity weakening friction allows a self-healing versus a cracklike mode of rupture, *Bull. Seism. Soc. Am.* **88,** 1466–1483.

Appendix A

The Bilateral Propagating Pulse: A Combined Mode Solution

A priori, any value of n may generate a proper mode n solution, for the Laplace domain function

$$ {}_n\tilde{V}(p) = A\sqrt{v_h^{-2} - v_r^{-2}}\,\frac{p^n}{v_h^{-n}\,(p^2 - v_r^{-2})^{3/2}\sqrt{v_h^{-2} - p^2}}, $$
$$ n = 0, 2, 4, \ldots . $$

In practice, it is found that only the first even modes ($n = 0$ and $n = 2$) yield acceptable solutions with proper behavior at the origin (no singularity in slip).

Reverse transform of ${}_0\tilde{V}(p)$ and ${}_2\tilde{V}(p)$ by Cagniard–de Hoop, following a contour going along the real axis in the upper right quarter plane, yields the following slip-rate functions:

$$ {}_0V(t/x) = A_0\,\frac{v_r^2\,(t/x)\sqrt{v_h^{-2} - (t/x)^2}}{\sqrt{(t/x)^2 - v_r^{-2}}} - A_0\,v_r^2\int_{v_r^{-1}}^{(t/x)}\frac{\sqrt{p^2 - v_r^{-2}}}{\sqrt{v_h^{-2} - p^2}}\,dp $$

$$ {}_2V(t/x) = A_2\,\frac{v_h^2\,(t/x)\sqrt{v_h^{-2} - (t/x)^2}}{\sqrt{(t/x)^2 - v_r^{-2}}} + A_2\,v_h^2\int_{v_r^{-1}}^{(t/x)}\frac{\sqrt{v_h^{-2} - p^2}}{\sqrt{p^2 - v_r^{-2}}}\,dp $$

in the interval $t\,v_h < x < t\,v_r$,

where both integral terms can be replaced by equivalent ellitpic integrals of the second kind second if wished, after a variable change:

$$ \int_{v_r^{-1}}^{(t/x)}\frac{\sqrt{p^2 - v_r^{-2}}}{\sqrt{v_h^{-2} - p^2}}\,dp = -\,\mathrm{Re}\left[\frac{i}{v_r}\,\mathbf{E}\left((t/x)\,v_h, \frac{v_r^2}{v_h^2}\right)\right] $$

$$ \int_{v_r^{-1}}^{(t/x)}\frac{\sqrt{v_h^{-2} - p^2}}{\sqrt{p^2 - v_r^{-2}}}\,dp = -\,\mathrm{Re}\left[\frac{i}{v_h}\,\mathbf{E}\left((t/x)\,v_r, \frac{v_h^2}{v_r^2}\right)\right]. $$

We remark that both modes are very similar, essentially built on the ratio of two square roots, $\sqrt{(t/x)^2 - v_r^{-2}}/\sqrt{v_h^{-2} - (t/x)^2}$. Such ratio also appears as the argument of the integral terms (the variable of integration p can indeed be considered as the very slowness t/x at earlier times). The essential difference between the two modes is that the square root ratio is inverted only inside the integral of ${}_0V$.

Both mode $n = 0$ and mode $n = 2$ solutions, taken by themselves, yield a constant residual slip-rate $V(t/x)$ after healing, a boundary condition hard to justify in a realistic situation. However, as suggested by J. Rice (personal comm., 2002), they can be combined together with an adequate coefficient yielding a unique solution that drops exactly to zero. Accordingly, we can group the first term of the two velocities and combine the two solutions to obtain.

$$ V(t/x) = (v_h^2\,A_0 + v_r^2\,A_2)\,\frac{v_r^2\,(t/x)\sqrt{v_h^{-2} - (t/x)^2}}{\sqrt{(t/x)^2 - v_r^{-2}}} - A_0\,v_r^2\int_{v_r^{-1}}^{(t/x)}\frac{\sqrt{p^2 - v_r^{-2}}}{\sqrt{v_h^{-2} - p^2}}\,dp + A_2\,v_h^2\int_{v_r^{-1}}^{(t/x)}\frac{\sqrt{v_h^{-2} - p^2}}{\sqrt{p^2 - v_r^{-2}}}\,dp. $$

In the first term of the slip rate, the real part vanishes after healing ($t/x > v_h^{-1}$). On the other hand, after healing time the integral terms will each have a constant, real residual value corresponding to the complete integral between bounds $p = v_r$ and $p = v_h$. The ratio of the two amplitude terms $\chi = A_2/A_0$, in order to allow a final zero slip rate after healing, should then satisfy

$$ \chi = A_2/A_0 = \frac{v_h^2\int_{v_r^{-1}}^{v_h^{-1}}\sqrt{v_h^{-2} - p^2}\,/\,\sqrt{p^2 - v_r^{-2}}\,dp}{v_r^2\int_{v_r^{-1}}^{v_h^{-1}}\sqrt{p^2 - v_r^{-2}}\,/\,\sqrt{v_h^{-2} - p^2}\,dp}. $$

These expressions include integral representations that can be easily integrated numerically for evaluation and plotting, once we fixed a rupture and a healing front velocity. The factor $\chi(v_r, v_h)$ is obtained by equating $V(t/x)$ to zero at any time $t > x/v_h$ after healing.

Stress can also be obtained in closed form (a singular term and the sum of several elliptic integrals), proceeding in similar fashion as for the unilateral pulse, except that a variable change $p \to 1/\zeta$ in the Laplace transform will facilitate transformation to the time–space domain through integration. We do not show any representation of slip, slip rate, or stress to avoid redundancy, since the resulting graphics are very similar to those obtained for the unilateral propagating pulse, with the obvious exception that they are symmetric with respect to the origin $x = 0$ in the present case. We note that a similar singularity in stress develops at the origin, because in this case, too, there is an abrupt rupture in slope of the slip function at the origin, which is in this case an even function of x.

We point out that, again, for the limit $x \to v_r t$ this solution has the exact same behavior as the classical crack.

Appendix B

The Pulse Propagating away from a Rigid Body

We note that a rather simple solution can be obtained also for

$$ \tilde{V}(p) = -\frac{p}{\sqrt{v_h^{-2} - p^2}\,(v_r^{-2} - p^2)^{3/2}}. $$

However, as remarked by J. Rice (personal comm., 2002), it turns out to correspond to an antisymmetric case, where the left half of the fault would be loaded loaded with a prestress $-\sigma_0$ while the right half of the fault is loaded with σ_0 stress of the opposite sign. Alternatively, it could be considered as a fracture nucleating right next to an infinitely rigid body and propagating away from it. There is no stress singularity at the origin in this case (slip being a linear uneven function of x close to the origin). It is clear that the latter solution is of limited practical interest.

Appendix C

Elliptic Integrals

The elliptic integrals of the first kind (F) and of the second kind (E) are defined (Gradshteyn and Ryzhik, 1965)

$$F(\phi,\ k)\ =\ \int_0^{\phi} d\theta\ (1\ -\ k^2\ \sin^2\theta)^{-1/2}$$

$$E(\phi,\ k)\ =\ \int_0^{\phi} d\theta\ (1\ -\ k^2\ \sin^2\theta)^{1/2}.$$

In the case of Kostrov's model, we run into elliptic integrals where $\phi\ =\ \arcsin\ p$ and $k\ =\ h^{-2}\ =\ v_r^2/\beta^2$. Let us make the following variable change,

$$\xi\ =\ \sin\theta,$$

in these expressions in order to obtain the equivalent integrals (see Gradshteyn and Ryzhik, 1965):

$$E(\arcsin\ p,\ h^{-2})\ =\ \int_0^{p} d\xi\ \frac{\sqrt{1\ -\ h^{-2}\xi^2}}{\sqrt{1\ -\ \xi^2}}$$

$$F(\arcsin\ p,\ h^{-2})\ =\ \int_0^{p} \frac{d\xi}{\sqrt{1\ -\ \xi^2}\ \sqrt{1\ -\ h^{-2}\xi^2}}.$$

The kernel of the two integrals is imaginary only in the range $1 < \xi < h$, so that the imaginary part of such integral functions is zero for $p < 1$ and a constant identical to its value at $p\ =\ h$ for values of $p \geq h$:

$$\begin{aligned}&\mathrm{Im}\ E(\arcsin\ p|_{p\geq h},\ h^{-2})\ =\ \text{Const.}\\ &=\ \mathrm{Im}\ E(\arcsin\ h,\ h^{-2})\ =\ \mathrm{Im}\ \mathbf{E}(h^{-2})\\ &=\ \mathrm{Im}\ \int_0^{h} \frac{\sqrt{1\ -\ h^{-2}\gamma^2}}{\sqrt{1\ -\ \gamma^2}}\ d\gamma\end{aligned}$$

$$\begin{aligned}&\mathrm{Im}\ F(\arcsin\ p|_{p\geq h},\ h^{-2})\ =\ \text{Const.}\\ &=\ \mathrm{Im}\ F(\arcsin\ h,\ h^{-2})\ =\ \mathrm{Im}\ \mathbf{F}(h^{-2})\\ &=\ \mathrm{Im}\ \int_0^{h} \frac{d\gamma}{\sqrt{1\ -\ h^{-2}\gamma^2}\sqrt{1\ -\ \gamma^2}},\end{aligned}$$

where the functions in bold are currently referred to as the complete elliptic integrals. For the normalization of the amplitude of Kostrov's slip-rate function, we need to compute the imaginary part of difference between the elliptic integrals:

$$\begin{aligned}I(h)\ &=\ \mathrm{Im}[\mathbf{F}(h^{-2})\ -\ \mathbf{E}(h^{-2})]\\ &=\ \mathrm{Im}\ \int_0^{h} \frac{\xi^2 d\xi}{h^2\ \sqrt{1\ -\ \xi^2}\sqrt{1\ -\ h^{-2}\xi^2}}.\end{aligned}$$

This integral can be evaluated in several ways. Kostrov (1964a) used contour integration in the complex ξ plane to convert the integral into one along the imaginary ξ axis. Here we derive an equivalent, simple closed form expression. First, note that in the given expression, the imaginary part is nonzero only for $1 < \xi < h$. Thus, after a variable change and some algebra, we can write

$$\mathrm{Im}\ \int_0^{h} \frac{\xi^2 d\xi}{h^2\sqrt{1\ -\ \xi^2}\sqrt{1\ -\ h^{-2}\xi^2}}\ =$$
$$\mathrm{Re}\ \int_0^{1/\sqrt{1-h^{-2}}} d\eta\ \frac{\sqrt{1\ -\ (1\ -\ h^{-2})\eta^2}}{\sqrt{1\ -\ \eta^2}}$$

We recognize, in the right-hand member, a complete integral $\mathbf{E}(1\ -\ h^{-2})$ so that, finally,

$$I(h)\ =\ \mathbf{E}(1\ -\ h^{-2}).$$

Istituto Nazionale di Geofisica e Vulcanologia
Roma, Italy
(S.N.)

Ecole Normale Superieure de Paris
Laboratoire de Géologie
Paris, France
(R.M.)

Manuscript received 27 March 2002.